Inorg. Chem. **2004**, *43*, 7508–7515

Effects of Pt···Pt Bonding, Anions, Solvate Molecules, and Hydrogen Bonding on the Self-Association of Chugaev's Cation, a Platinum Complex with a Chelating Carbene Ligand

Jay R. Stork, Marilyn M. Olmstead, and Alan L. Balch*

Department of Chemistry, University of California, Davis, California 95616

Received June 14, 2004

Five salts, $[(C_4H_9N_4)Pt^{II}(CNCH_3)_2](BPh_4)\cdot CH_3OH$, $[(C_4H_9N_4)Pt^{II}(CNCH_3)_2](PF_6)\cdot CH_2Cl_2$, $[(C_4H_9N_4)Pt^{II}(CNCH_3)_2]Cl\cdot 4H_2O$, $[(C_4H_9N_4)Pt^{II}(CNCH_3)_2]Br\cdot 3.5H_2O$, and $[(C_4H_9N_4)Pt^{II}(CNCH_3)_2]Cl\cdot 0.1H_2O$, have been crystallized and examined by single crystal X-ray diffraction. While the internal structure of the cation is similar in all salts, the interactions between cations vary in the different salts. Yellow $[(C_4H_9N_4)Pt^{II}(CNCH_3)_2](BPh_4)\cdot CH_3OH$ and red $[(C_4H_9N_4)Pt^{II}(CNCH_3)_2](PF_6)$ form face-to-face dimers with Pt···Pt separations of 3.6617(6) and 3.340(2) Å, respectively. In the latter, hydrogen bonding of the chelating ligand to adjacent anions facilitates the close approach of pairs of cations. The salts $[(C_4H_9N_4)Pt^{II}(CNCH_3)_2]Cl\cdot 4H_2O$, $[(C_4H_9N_4)Pt^{II}(CNCH_3)_2]Br\cdot 3.5H_2O$, and $[(C_4H_9N_4)Pt^{II}(CNCH_3)_2]Cl\cdot 0.1H_2O$ form columnar structures with Pt···Pt separations that range from 3.2514(5) to 3.5643(6) Å. The water molecules and anions surround these columns and form bridges between neighboring columns. The electronic spectra of aqueous solutions of $[(C_4H_9N_4)Pt^{II}(CNCH_3)_2]Cl\cdot 4H_2O$ show spectral changes upon increasing concentrations of the platinum complex that are indicative of the formation of a dimer in solution with an equilibrium constant for dimerization of 23(1).

Introduction

A number of structural studies have shown that outer sphere coordination effects including cation/anion interactions, solvent effects, and hydrogen bonding can influence the self-association and metal−metal bonding in ionic complexes of four-coordinate platinum(II) and two-coordinate gold(I). These factors also influence the complexes' spectroscopic properties, which are frequently connected to the formation of aggregates where the metal ions interact by overlap of the filled d_{z^2} orbitals and of the empty p_z orbitals.

For example, salts of $[Pt^{II}(CN)_4]^{2-}$ are well-known to self-associate to form stacks in which the Pt···Pt separations, which range from 3.09 to 3.71 Å, and the spectroscopic properties are sensitive to the cations involved and the hydration state of the crystals.[1] The crystalline double salts, $[Pt^{II}(CNR)_4][Pt^{II}(CN)_4]$, display vapochromic behavior; that is, they undergo color changes when exposed to the vapors of volatile organic compounds.[2−4] These salts contain stacks of alternating $[Pt^{II}(CNR)_4]^{2+}$ and $[Pt^{II}(CN)_4]^{2-}$ ions with overlap of the filled, out-of-plane d_{z^2} orbitals on platinum running along the stacks. The color changes have been shown to be correlated with hydrogen bonding interactions between the adsorbed organic molecules and the cyano groups of the $[Pt^{II}(CN)_4]^{2-}$ ions.[4]

Scheme 1

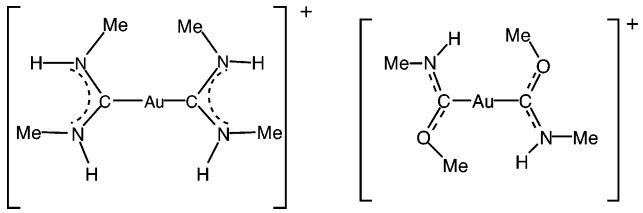

$[Au\{C(NHMe)_2\}_2]^+$ $[Au\{C(OMe)NMeH\}_2]^+$

In another case, the cation $[Au^I\{C(NHMe)_2\}_2]^+$, whose structure is shown in Scheme 1, forms different types of aggregates depending upon the anion present. When the

* To whom correspondence should be addressed. E-mail: albalch@ucdavis.edu.

(1) Williams, J. M.; Schultz, A. J.; Underhill, A. E.; Carneiro, K. In *Extended Linear Chain Compounds*; Miller, J. S., Ed.; Plenum Press: New York, 1982; Vol 1, p 73.
(2) Daws, C. A.; Exstrom, C. L.; Sowa, J. R.; Mann, K. R. *Chem. Mater.* **1997**, *9*, 363.
(3) Buss, C. E.; Anderson, C. E.; Pomije, M. K.; Lutz, C. M.; Britton, D.; Mann, K. R. *J. Am. Chem. Soc.* **1998**, *120*, 7783.
(4) Exstrom, C. L.; Pomije, M. K.; Mann, K. R. *Chem. Mater.* **1998**, *10*, 942.

10.1021/ic049226j CCC: $27.50
Published on Web 10/22/2004

Scheme 2

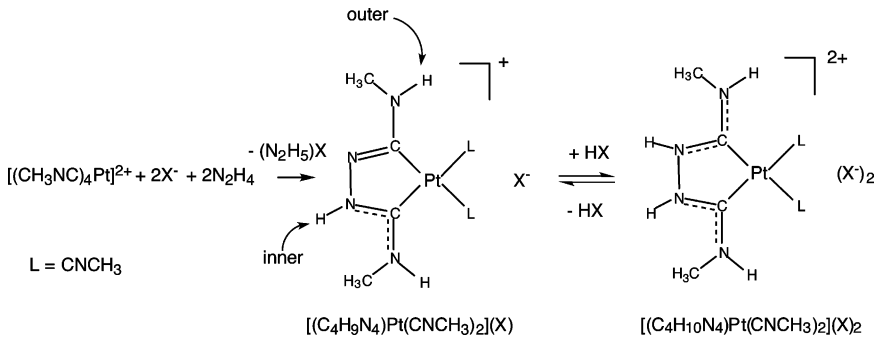

anion is chloride or bromide, the cations form dimers through Au···Au interactions, and the anions form hydrogen bonds with the ligands.[5] On the other hand, the hexafluorophosphate salt of $[Au^{I}\{C(NHMe)_2\}_2]^+$ forms a linear stack with a Au···Au separation of 3.1882(1) Å.[6] These stacks are reinforced by the anions which form hydrogen bonds with adjacent cations in a column. The tetrafluoroborate salt of $[Au^{I}\{C(NHMe)_2\}_2]^+$ assumes another stacked structure where the Au···Au separations are larger (3.4615(2) Å), and the cations have an eclipsed rather than staggered orientation. The cation $[Au^{I}\{C(OMe)NMeH\}_2]^+$ shown in Scheme 1 has been crystallized in three environments.[7] Thus, the chloroform solvate, $[Au^{I}\{C(OMe)NMeH\}_2][C_7Cl_2NO_3]\cdot CHCl_3$, contains the cation as an isolated monomer, while unsolvated $[Au^{I}\{C(OMe)NMeH\}_2][C_7Cl_2NO_3]$ contains pairs of cations in eclipsed orientations that are linked by a single Au···Au interaction with a 3.1955(3) Å separation between the gold centers. In $[Au^{I}\{C(OMe)NMeH\}_2][O_2CCF_3]$, the cations form infinite, nearly linear chains (Au···Au···Au angle, 172.209(7)°) that have the gold centers 3.27797(15) Å apart. In a final example, hydrogen bonding to cations affects the ways in which $[Au(CN)_2]^-$ ions self-associate in the solid state.[8]

In this paper, we examine the outer sphere coordination effects on the supramolecular structure of a related platinum complex. Treatment of $[Pt^{II}(CNCH_3)_4]^{2+}$ with hydrazine results in the formation of the orange cation $[(C_4H_9N_4)Pt^{II}(CNCH_3)_2]^+$ as shown in Scheme 2.[9−11] This cation has structural elements similar to those of the gold complexes shown in Scheme 1. Previous work has established the molecular structure of the cation, $[(C_4H_9N_4)Pt^{II}(CNCH_3)_2]^+$, but has not dealt with the supramolecular aspects of the solid state structures of these complexes. It has been noted that these salts display a range of colors that appear to be indicative of structural variations. For example, $[(C_4H_9N_4)Pt^{II}(CNCH_3)_2]Cl\cdot 4H_2O$ was reported to be red but change to green upon dehydration, and the azide salt was described as blue.[9] Here we present work on the structures of several salts of $[(C_4H_9N_4)Pt^{II}(CNCH_3)_2]^+$ and on the spectroscopic properties of this cation in solution and in the solid state.

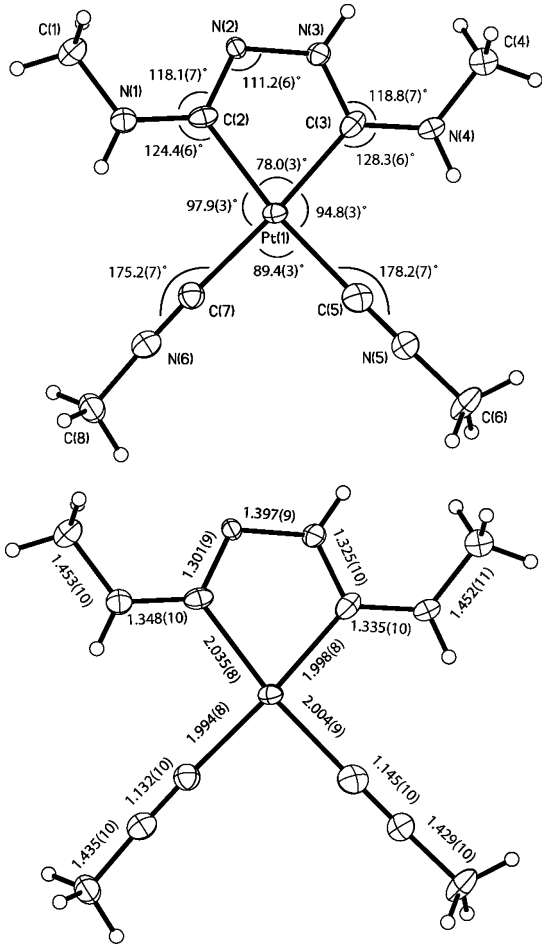

Figure 1. Drawing of the cation $[(C_4H_9N_4)Pt^{II}(CNCH_3)_2]^+$ in $[(C_4H_9N_4)Pt^{II}(CNCH_3)_2](BPh_4)\cdot CH_3OH$ that shows selected distances (in Å) and angles (in deg) within the cation.

Results

Studies of the Solid State Structures. The salts, $[(C_4H_9N_4)Pt^{II}(CNCH_3)_2](BPh_4)\cdot CH_3OH$, $[(C_4H_9N_4)Pt^{II}(CNCH_3)_2](PF_6)\cdot CH_2Cl_2$, $[(C_4H_9N_4)Pt^{II}(CNCH_3)_2]Cl\cdot 4H_2O$, $[(C_4H_9N_4)Pt^{II}(CNCH_3)_2]Cl\cdot 0.1H_2O$, and $[(C_4H_9N_4)Pt^{II}(CNCH_3)_2]Br\cdot 3.5H_2O$, have been crystallized and examined by single crystal X-ray diffraction. Crystal data are given in Table 1. Unfortunately,

(5) White-Morris, R. L.; Olmstead, M. M.; Jiang, F.; Balch, A. L. *Inorg. Chem.* **2002**, *41*, 2313.
(6) White-Morris, R. L.; Olmstead, M. M.; Jiang, F.; Tinti, D. S.; Balch, A. L. *J. Am. Chem. Soc.* **2002**, *124*, 2327.
(7) Jiang, F.; Olmstead, M. M.; Balch, A. L. *J. Chem. Soc., Dalton Trans.* **2000**, 4098.
(8) Stender, M.; Olmstead, M. M.; Balch, A. L.; Rios, D.; Attar, S. *J. Chem. Soc., Dalton Trans.* **2003**, 4282.
(9) Tshugajeff (Chugaev), L.; Skanavii-Grigorieva, M.; Posnlak, A. *Z. Anorg. Allg. Chem.* **1925**, 37.
(10) Burke, A.; Balch, A. L.; Enemark, J. H. *J. Am. Chem. Soc.* **1970**, *92*, 2555.
(11) Butler, W. M.; Enemark, J. H.; Parks, J.; Balch, A. L. *Inorg. Chem.* **1973**, *12*, 451.

Table 1. Crystal Data and Data Collection Parameters

	$[(C_4H_9N_4)Pt^{II}(CNCH_3)_2](BPh_4)\cdot CH_3OH$	$[(C_4H_9N_4)Pt^{II}(CNCH_3)_2](PF_6)\cdot CH_2Cl_2$	$[(C_4H_9N_4)Pt^{II}(CNCH_3)_2]Cl\cdot 4H_2O$	$[(C_4H_9N_4)Pt^{II}(CNCH_3)_2]Cl\cdot 0.10H_2O$	$[(C_4H_9N_4)Pt^{II}(CNCH_3)_2]Br\cdot 3.5H_2O$
formula	$C_{33}H_{39}BN_6OPt$	$C_9H_{17}Cl_2F_6N_6Pt$	$C_8H_{23}ClN_6O_4Pt$	$C_8H_{15.2}ClN_6O_{0.10}Pt$	$C_8H_{22}BrN_6O_{3.5}Pt$
fw	741.60	618.12	497.86	427.60	533.32
color, habit	yellow plate	red block	red needle	red/green needle	red block
cryst syst	monoclinic	monoclinic	monoclinic	monoclinic	triclinic
space group	$P2_1/c$	$P2/n$	$P2_1$	$C2/c$	$P\bar{1}$
a, Å	11.0167(12)	10.681(3)	6.6678(10)	17.4705(14)	6.6625(13)
b, Å	11.0796(12)	19.021(6)	19.959(3)	12.3940(10)	12.215(3)
c, Å	27.931(3)	20.620(7)	12.5422(18)	13.0137(10)	21.932(5)
α, deg	90	90	90	90	79.086(6)
β, deg	112.096(2)	90.446(7)	93.155(3)	113.7150(10)	84.987(7)
γ, deg	90	90	90	90	75.038(5)
V, Å^3	3158.8(6)	4189(2)	1666.6(4)	2579.9(4)	1691.9(6)
Z	4	8	4	8	4
T, K	90(2)	90(2)	90(2)	90(2)	90(2)
λ, Å	0.71073 (Mo Kα)	0.71073 (Mo Kα)	0.71073 (Mo Kα)	0.71073 (Mo Kα)	0.71073 (Mo Kα)
ρ, g/cm^3	1.559	1.960	1.984	2.201	2.094
μ, mm^{-1}	4.478	7.080	8.600	11.070	10.671
R1[a] (obsd data)	0.039	0.082	0.020	0.016	0.036
wR2 (all data, F^2 refinement)	0.099	0.192	0.044	0.038	0.080

[a] $R1 = \frac{\sum||F_o| - |F_c||}{\sum|F_o|}$; $wR2 = \sqrt{\frac{\sum[w(F_o^2 - F_c^2)^2]}{\sum[w(F_o^2)^2]}}$

the blue azide salt undergoes decomposition before suitable crystals could be obtained. Although the structure of the cation is nearly invariant within these crystals, the interactions between cations vary in the different salts as will be described. In particular, note that there are two types of N−H groups referred to as "inner" and "outer" as shown in Scheme 2. Both types of N−H groups are extensively involved in hydrogen bonding in the crystals.

$[(C_4H_9N_4)Pt^{II}(CNCH_3)_2](BPh_4)\cdot CH_3OH$. The asymmetric unit of this yellow salt consists of a cation, an anion, and a methanol molecule, each in general positions. Figure 1 shows a drawing of the cation with selected interatomic distances and angles. The cation is nearly planar, and its structure is similar to those of related complexes such as the palladium analogue of $[(C_4H_9N_4)Pt^{II}(CNCH_3)_2]^+$ reported earlier.[11]

Figure 2 shows the Pt···Pt interactions between the cations and the hydrogen bonding between the cations and methanol molecules. The cations form dimers about a crystallographic center of symmetry. The Pt···Pt separation within a dimer is 3.6621(7) Å, which is the longest such distance encountered within the group of salts reported here. Each dimer is connected to another dimer through hydrogen bonds to methanol molecules. The set of two cations and two methanol molecules also packs about another center of symmetry. Each methanol molecule donates a hydrogen bond to the deprotonated nitrogen of one cation and accepts a hydrogen bond from the inner N−H group of another cation. There are no unusually close contacts between these components of the structure and the anions.

$[(C_4H_9N_4)Pt^{II}(CNCH_3)_2](PF_6)\cdot CH_2Cl_2$. This compound crystallizes as a mixture of red blocks and plates. The asymmetric unit contains two cations, in general positions, an anion in a general position, two-half-anions in special positions, and four sites for dichloromethane molecules with disorder and fractional occupancy. The geometry of each of the individual cations is very similar to that shown in Figure 1.

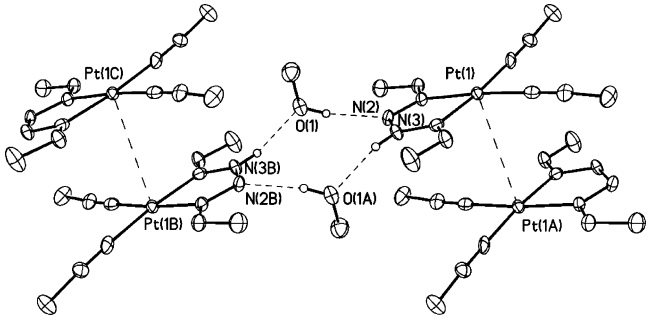

Figure 2. View of the supramolecular structure of $[(C_4H_9N_4)Pt^{II}(CNCH_3)_2](BPh_4)\cdot CH_3OH$ showing the interactions between pairs of cations and between cations and methanol molecules. The positions of the anions are not shown.

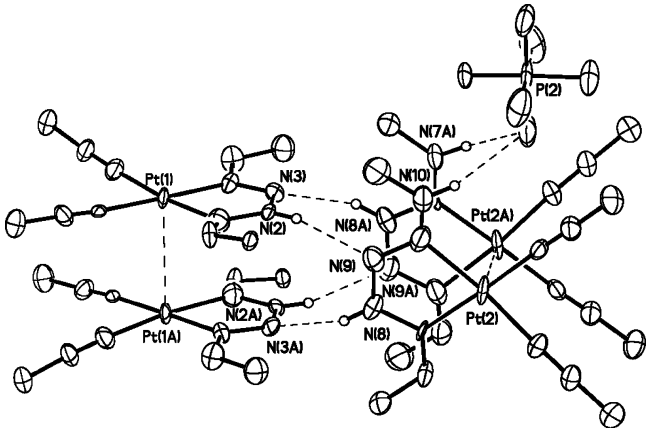

Figure 3. Drawing showing the interactions between four cations in $[(C_4H_9N_4)Pt^{II}(CNCH_3)_2](PF_6)\cdot CH_2Cl_2$. One anion, which is hydrogen-bonded to a pair of cations, is also shown. There are three other anions that surround this unit in identical positions, but for clarity these are not shown.

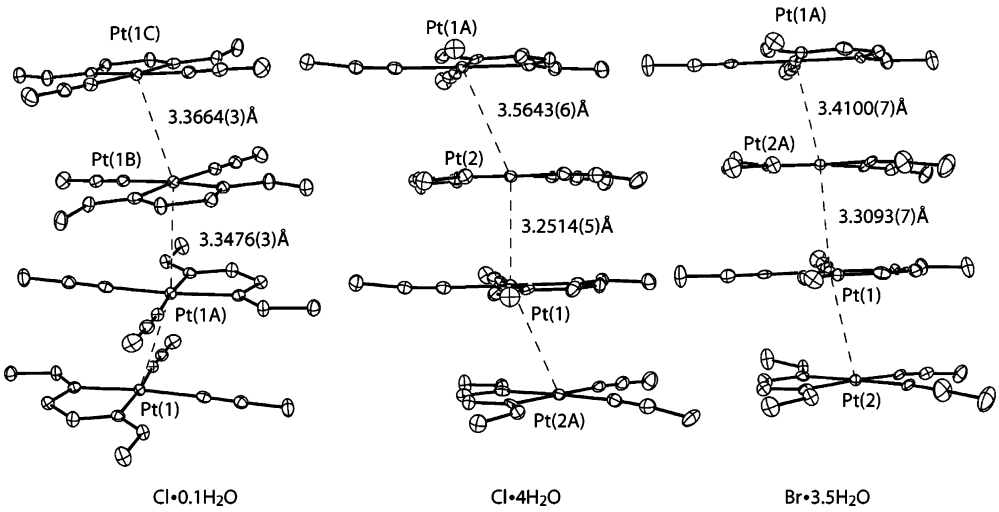

Figure 4. Drawings of the columns of cations in $[(C_4H_9N_4)Pt^{II}(CNCH_3)_2]Cl\cdot 4H_2O$, $[(C_4H_9N_4)Pt^{II}(CNCH_3)_2]Cl\cdot 0.1H_2O$, and $[(C_4H_9N_4)Pt^{II}(CNCH_3)_2]Br\cdot 3.5H_2O$.

Four cations form a cluster that involves hydrogen bonding and Pt···Pt interactions as seen in Figure 3. Pairs of cations form eclipsed dimers with a Pt(1)···Pt(1A) separation of 3.340(2) Å in one dimer and a Pt(2)···Pt(2A) separation of 3.398(2) Å in the other dimer. One dimer is then connected to another dimer through hydrogen bonds. These hydrogen bonds occur between the inner N−H group of the chelating ligand on one cation and the deprotonated nitrogen atom of the chelating ligand on an adjacent cation. Four hexafluorophosphate ions surround this cluster and are hydrogen bond receptors from four of the outer N−H groups of the chelating ligands. In order to keep the figure legible, only one of these hexafluorophosphate ions is shown in Figure 3.

$[(C_4H_9N_4)Pt^{II}(CNCH_3)_2]Cl\cdot 4H_2O$. There are two cations, two chloride ions, and eight water molecules in the asymmetric unit of the bright red crystals of this salt. The two crystallographically distinct cations pack alternately to form columns that run parallel to the crystallographic *a* axis. A portion of one such column is shown in Figure 4. In these columns there are two different Pt···Pt separations. The Pt(1)···Pt(2) distance is 3.2514(5) Å while the Pt(1)···Pt(2A) distance is 3.5643(6) Å. The columns are not linear. The Pt(2)···Pt(1)···Pt(2A) angle is 156.056(9)°.

The chloride ions and water molecules form a complex network that connects cations within a column and cations in adjacent columns as shown in Figure 5. Within this array, four water molecules form a chain of hydrogen bonds that run from the outer N−H group of the chelating ligand on one cation to the deprotonated inner nitrogen atom of another cation in a different chain of cations. The chloride ion is hydrogen bonded to three water molecules and to the inner N−H group of one cation. Each of the three water molecules surrounding the chloride ion forms a hydrogen bond to a different cation.

Part A of Figure 6 shows the environment of Cl(2), which makes hydrogen bonds to the outer N−H group of one cation and to two water molecules. These two water molecules also from hydrogen bonds to a second cation.

$[(C_4H_9N_4)Pt^{II}(CNCH_3)_2]Cl\cdot 0.1H_2O$. Upon dehydration, red crystals of $[(C_4H_9N_4)Pt^{II}(CNCH_3)_2]Cl\cdot 4H_2O$ darken and

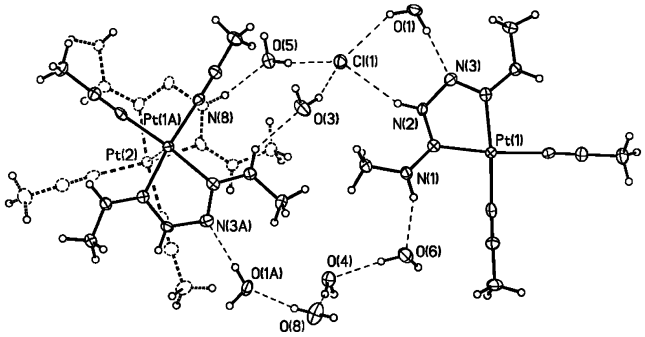

Figure 5. View of the hydrogen bonded network between three cations in two different columns in crystalline $[(C_4H_9N_4)Pt^{II}(CNCH_3)_2]Cl\cdot 4H_2O$. The cation containing Pt(2) is shown with dashed lines to emphasize the fact that it is below the cation containing Pt(1A).

acquire a metallic green sheen. This process is accompanied with a loss of crystallinity. However, a nearly anhydrous form can be obtained by recrystallization of a sample of the dehydrated complex from dimethyl sulfoxide solution with addition of dichloromethane. This process yields reddish purple needles of $[(C_4H_9N_4)Pt^{II}(CNCH_3)_2]Cl\cdot 0.1H_2O$ that have a metallic green sheen.

There are one cation and one anion in the asymmetric unit. Additionally, there is a partially occupied site which has been assigned as a water molecule with 0.10 fractional occupancy. The cations are arranged in helical columns with short Pt···Pt contacts as seen in Figure 4. These columns are situated around the crystallographic *c* axis. The two different Pt···Pt distances are 3.3476(3) Å for Pt(1)···Pt(1A) and 3.3664(3) Å for Pt(1)···Pt(1B). Again, the chain of platinum atoms is bent with a Pt(1A)···Pt(1)···Pt(1B) angle of 159.359(4)°.

Comparison of the structures of $[(C_4H_9N_4)Pt^{II}(CNCH_3)_2]$-$Cl\cdot 4H_2O$ and $[(C_4H_9N_4)Pt^{II}(CNCH_3)_2]Cl\cdot 0.1H_2O$ reveals that the columns of platinum cations are less widely spaced in the less hydrated form. Thus, the shortest nonbonded Pt-to-Pt distance between adjacent columns is 10.912 Å in $[(C_4H_9N_4)Pt^{II}(CNCH_3)_2]Cl\cdot 4H_2O$ while that distance is 9.323 Å in $[(C_4H_9N_4)Pt^{II}(CNCH_3)_2]Cl\cdot 0.1H_2O$. This difference is consistent with the location of the water molecules which surround the cation in a lateral fashion in $[(C_4H_9N_4)Pt^{II}$-

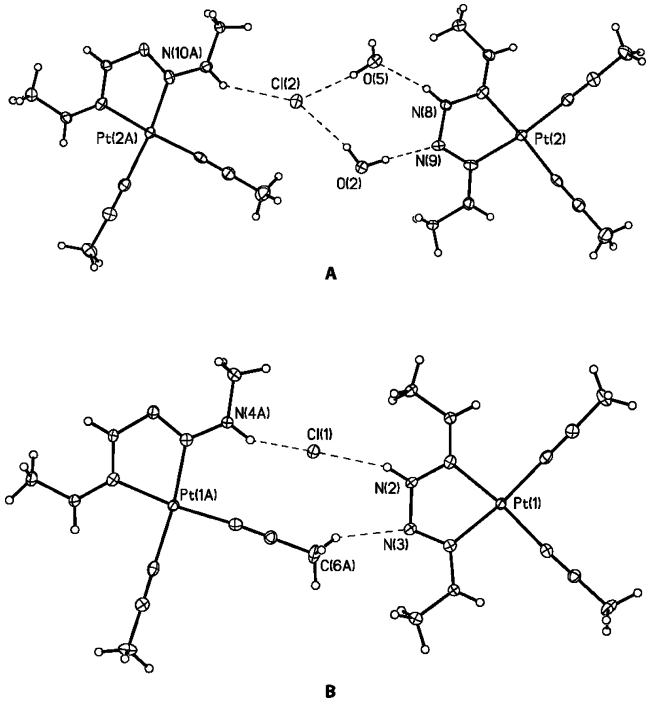

Figure 6. Comparison of related regions of the structures of A, $[(C_4H_9N_4)Pt^{II}(CNCH_3)_2]Cl{\cdot}4H_2O$, and B, $[(C_4H_9N_4)Pt^{II}(CNCH_3)_2]Cl{\cdot}0.1H_2O$.

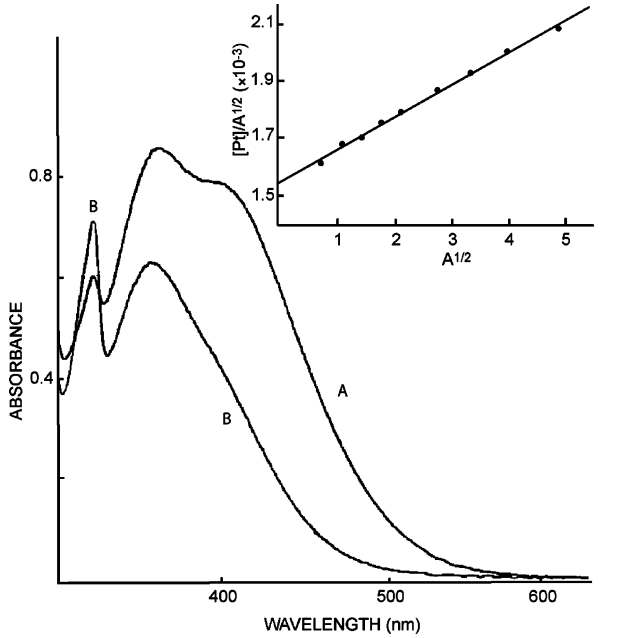

Figure 7. Electronic spectra of solutions of $[(C_4H_9N_4)Pt^{II}(CNCH_3)_2]Cl{\cdot}4H_2O$ in aqueous 1.00 M potassium phosphate, pH 7.20. Trace A: 2.44×10^{-3} total platinum concentration, 1.00 mm cells. Trace B: 2.44×10^{-4} total platinum concentration, 1.00 cm cells. The inset shows a plot of $[Pt]/A^{1/2}$ versus $A^{1/2}$.

$(CNCH_3)_2]Cl{\cdot}4H_2O$ and are nearly absent in $[(C_4H_9N_4)Pt^{II}(CNCH_3)_2]Cl{\cdot}0.1H_2O$. A relevant comparison is shown in Figure 6, which compares related sections of the structures of $[(C_4H_9N_4)Pt^{II}(CNCH_3)_2]Cl{\cdot}4H_2O$ in A and $[(C_4H_9N_4)Pt^{II}(CNCH_3)_2]Cl{\cdot}0.1H_2O$ in B. In $[(C_4H_9N_4)Pt^{II}(CNCH_3)_2]Cl{\cdot}4H_2O$, one cation is connected laterally through hydrogen bonds to two water molecules which are hydrogen bonded to a chloride ion. That chloride ion makes another hydrogen bond to the outer N−H group of a different cation. The distance between the platinum atoms in the different cations in this array is 12.8423(13) Å. In contrast, in $[(C_4H_9N_4)Pt^{II}(CNCH_3)_2]Cl{\cdot}0.1H_2O$ the two water molecules are absent, and the intervening chloride ion makes hydrogen bonds to the inner N−H group of one cation and the outer N−H group of another. In this arrangement, the distance between the two platinum atoms of neighboring cations is 9.9263(5) Å.

$[(C_4H_9N_4)Pt^{II}(CNCH_3)_2]Br{\cdot}3.5H_2O$. The asymmetric unit of this red salt consists of two cations in general positions, one fully occupied anion site Br(1) in a general position, one anion site Br(2) located at a center of symmetry that accounts for one-half of a bromide ion, and a third site Br(3) in a general position with a fractional occupancy of 0.5, and seven water molecules. The cations are arranged in columns which are remarkably similar to those in $[(C_4H_9N_4)Pt^{II}(CNCH_3)_2]Cl{\cdot}4H_2O$, although the two salts are not isostructural. Figure 4 allows the two chains to be compared. The Pt(1)···Pt(2) distance in $[(C_4H_9N_4)Pt^{II}(CNCH_3)_2]Br{\cdot}3.5H_2O$ is 3.3093(7) Å, and the Pt(1)···Pt(2A) distance is 3.4100(7) Å. The stacking of the cations produces a bent chain of platinum atoms with a Pt(2)···Pt(1)···Pt(2A) angle of 165.090(13)°. As with $[(C_4H_9N_4)Pt^{II}(CNCH_3)_2]Cl{\cdot}4H_2O$, the water molecules and bromide ions form hydrogen-bonded arrays that radiate laterally from the cation and connect cations in neighboring chains. Examples are shown in the Supporting Information as Figures S1, S2, and S3.

Spectroscopic Properties. The electronic spectra of aqueous solutions of $[(C_4H_9N_4)Pt^{II}(CNCH_3)_2]Cl{\cdot}4H_2O$ do not obey Beer's Law. This is apparent from the data shown in Figure 7. Concentrated solutions have a peak at 395 nm that is absent in dilute solutions and in solutions of $[(C_4H_9N_4)Pt^{II}(CNCH_3)_2]Cl{\cdot}4H_2O$ in nonaqueous solvents such as acetone, acetonitrile, and *N*,*N*-dimethylformamide. In order to identify the degree of aggregation responsible for the low energy absorption, the concentration dependence of the absorptivity has been examined. Data obtained at 480 nm have been used in order to minimize overlap between the two absorption bands. For a system undergoing the monomer−dimer equilibrium shown in eq 1, the absorbance is related to the total platinum concentration, [Pt], by eq 2, where A is the measured absorbance (in this case at 480 nm) standardized to a 1 cm path length, K is the equilibrium constant for eq 1, and ϵ is the molar extinction coefficient (at 480 nm) of the dimer. The derivation of this equation is given in the Supporting Information.

$$2[(C_4H_9N_4)Pt^{II}(CNCH_3)_2]^+ \rightleftharpoons [(C_4H_9N_4)Pt^{II}(CNCH_3)_2]_2^{2+} \quad (1)$$

$$\left[\frac{[Pt]}{A^{1/2}}\right] = \left[\frac{1}{(\epsilon K)^{1/2}}\right] + \left[\frac{2A^{1/2}}{\epsilon}\right] \quad (2)$$

A plot of $[Pt]/A^{1/2}$ versus $A^{1/2}$ for $[(C_4H_9N_4)Pt^{II}(CNCH_3)_2]Cl{\cdot}4H_2O$ is shown in the inset to Figure 7. The linearity of the plot indicates that the low energy absorption results from a dimeric species. Analysis of these data gives $K = 23(1)$ with $\epsilon_{480} = 18(1) \times 10^3$ for this system in 1.00 M aqueous potassium phosphate buffer at pH 7.20. The structure of the

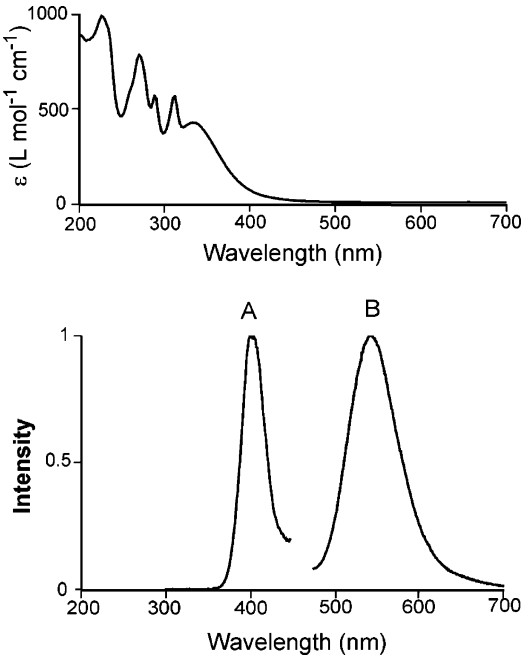

Figure 8. Electronic absorption (A), emission (B), and excitation (C) spectra from a solution of $[(C_4H_9N_4)Pt^{II}(CNCH_3)_2]Cl\cdot 4H_2O$ in aqueous 1.00 M potassium phosphate buffer, pH 3.0. The species responsible for the spectra is the dication, $[(C_4H_{10}N_4)Pt^{II}(CNCH_3)_2]^{2+}$.

dimeric species found in solution is probably closely similar to that of the dimeric unit identified in the X-ray crystallographic structures of $[(C_4H_9N_4)Pt^{II}(CNCH_3)_2](BPh_4)\cdot CH_3OH$ and $[(C_4H_9N_4)Pt^{II}(CNCH_3)_2](PF_6)$.

The ionic strength of the solution plays a significant role in the degree of association. Qualitative observations indicate that the equilibrium constant for dimerization is lower for lower ionic strength solutions.

Since $[(C_4H_9N_4)Pt^{II}(CNCH_3)_2]Cl\cdot 4H_2O$ is a weak base, pH control is also important. In acidic solution, $[(C_4H_9N_4)Pt^{II}(CNCH_3)_2]Cl\cdot 4H_2O$ becomes protonated, and its absorption spectrum is drastically altered. Relevant data are shown in Figure 8. In an aqueous solution buffered at pH 3, the dication $[(C_4H_9N_4)Pt^{II}(CNCH_3)_2]^{2+}$ is formed. This dication obeys Beer's Law over the concentration range 12−0.5 mM. Protonation of $[(C_4H_9N_4)Pt^{II}(CNCH_3)_2]^{+}$ to form $[(C_4H_9N_4)Pt^{II}(CNCH_3)_2]^{2+}$ inhibits the ability of the complex to self-associate, since the Coulombic repulsion between dications is greater than the repulsion between monocations.

Solutions of $[(C_4H_9N_4)Pt^{II}(CNCH_3)_2]Cl\cdot 4H_2O$ are not luminescent, but they become luminescent at low pH due to the formation of the dication, $[(C_4H_{10}N_4)Pt^{II}(CNCH_3)_2]^{2+}$. The emission and excitation spectra are shown in Figure 8.

The absorption spectra taken on the solid salts show low energy transitions that are a result of the Pt···Pt interactions that are present in the solid. Thus, $[(C_4H_9N_4)Pt^{II}(CNCH_3)_2](BPh_4)\cdot CH_3OH$ exhibits an absorption at 410 nm, which is not too different from the dimer absorption band seen in the solution spectra. For the other solids with shorter Pt···Pt contacts and in some cases more extended structures, this absorption occurs at lower energies: $[(C_4H_9N_4)Pt^{II}(CNCH_3)_2](PF_6)\cdot CH_2Cl_2$, 510 nm; $[(C_4H_9N_4)Pt^{II}(CNCH_3)_2]Cl\cdot 4H_2O$, 480 nm; $[(C_4H_9N_4)Pt^{II}(CNCH_3)_2]Cl\cdot 0.1H_2O$, 530 nm; and $[(C_4H_9N_4)Pt^{II}(CNCH_3)_2]Br\cdot 3.5H_2O$, 510 nm.

Data from the infrared spectra of these crystals are given in the Experimental Section. These spectra all show isocyanide absorptions in the 2261−2243 cm^{-1} region and are consistent with previously reported infrared spectra for Chugaev's red cation.[10,11,16]

Discussion

The results presented here demonstrate the proclivity of the cation, $[(C_4H_9N_4)Pt^{II}(CNCH_3)_2]^{+}$, to self-associate into various aggregates through direct Pt···Pt interactions with significant hydrogen bonding playing a major role in the structural organization. A recent review highlights the range of hydrogen bonding possibilities that exist in transition metal complexes.[12] It is interesting to note that the four-coordinate cation, $[(C_4H_9N_4)Pt^{II}(CNCH_3)_2]^{+}$, prefers self-association over traditional coordination of potentially coordinating anions such as chloride and bromide.

The nature of the self-association of $[(C_4H_9N_4)Pt^{II}(CNCH_3)_2]^{+}$ and the Pt···Pt distances involved vary significantly in the salts examined here. The weakest Pt···Pt interactions occur in the face-to-face dimer in $[(C_4H_9N_4)Pt^{II}(CNCH_3)_2](BPh_4)\cdot CH_3OH$ where the cations are associated in a centrosymmetric fashion with a Pt···Pt distance of 3.6617(6) Å. Red $[(C_4H_9N_4)Pt^{II}(CNCH_3)_2](PF_6)\cdot CH_2Cl_2$ also forms a face-to-face dimer but one with a shorter Pt···Pt separation of 3.340(2) Å. In the latter case, hydrogen bonding involving the outer N−H groups of the chelating ligands and the anions facilitates the close approach of the pairs of cations. Crystals of $[(C_4H_9N_4)Pt^{II}(CNCH_3)_2]Cl\cdot 4H_2O$, $[(C_4H_9N_4)Pt^{II}(CNCH_3)_2]Cl\cdot 0.1H_2O$, and $[(C_4H_9N_4)Pt^{II}(CNCH_3)_2]Br\cdot 3.5H_2O$ all form extended columnar structures with Pt···Pt separations that range from 3.2514(5) to 3.5643(6) Å. These columns are surrounded by anions and water molecules which produce hydrogen-bonded networks of interactions that connect adjacent cations as seen, for example, in Figure 5. Because of the variation in the nature of the mode of self-association of $[(C_4H_9N_4)Pt^{II}(CNCH_3)_2]^{+}$, there is no simple correlation between the low-energy absorption bands seen for these salts and the Pt···Pt distances.

Self-association of $[(C_4H_9N_4)Pt^{II}(CNCH_3)_2]^{+}$ also occurs in concentrated aqueous solutions, and a dimeric species can be identified by a characteristic absorption band at 395 nm. Examination of the spectral changes that occur when the concentration of $[(C_4H_9N_4)Pt^{II}(CNCH_3)_2]^{+}$ is varied has allowed us to measure the equilibrium constant ($K = 23(1)$) for the dimerization given in eq 1. These measurements demonstrate that a well-defined dimer exists in aqueous solution and that the formation of this dimer is effected by the pH of the solution. Protonation of $[(C_4H_9N_4)Pt^{II}(CNCH_3)_2]^{+}$ produces a dication which no longer shows evidence of self-association but which is luminescent in

(12) Brammer, L. *Dalton Trans.* **2003**, 3145.
(13) Mann, K. R.; Gordon, J. G., II; Gray, H. B. *J. Am. Chem. Soc.* **1975**, *97*, 3553.
(14) Martellaro, P. J.; Abbott, E. H. *Inorg. Chem.* **2000**, *39*, 1878.
(15) Lai, S.-W.; Chan, M. C. W.; Wang, Y.; Lam, H.-W.; Peng, S.-M.; Che, C.-M. *J. Organomet. Chem.* **2001**, *617*−*618*, 133.
(16) Lai, S.-W.; Cheung, K.-K.; Chan, M. C.-W.; Che, C.-M. *Angew. Chem., Int. Ed.* **1998**, *37*, 182.

Scheme 3

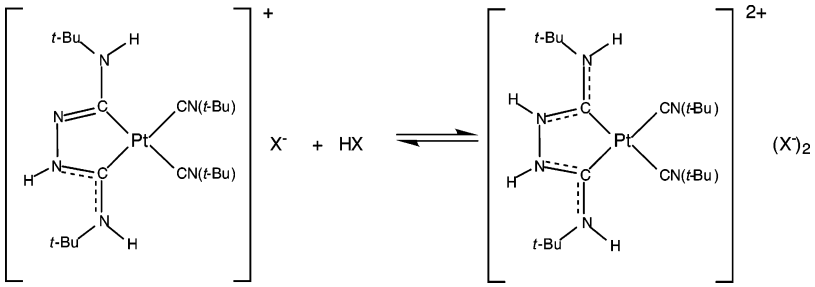

solution at room temperature. Unfortunately, there are few quantitative data regarding the equilibrium constants for self-association of d^8 metal complexes of the type discussed here. Self-association of complexes of the type $[Rh^I(CNR)_4]^+$ is well-known.[13] The equilibrium constant for self-association of $[Rh^I(CNPh)_4](PF_6)$ in acetonitrile has been reported as 16-(1),[13] a value remarkably close to that reported here for another monoanion in aqueous solution. Equilibrium constants have also been measured for the association between the d^8 complexes $[Pt^{II}(CNEt)_4]^{2+}$ and $[Pt(CN)_4]^{2-}$.[14] However, in this case Coulombic attraction rather than Coulombic repulsion is present. Consequently, the equilibrium constant is large, 5.1×10^5 in water at 22 °C.[14]

Recent work on similar complexes derived from *tert*-butyl isocyanide has uncovered luminescence in a cation analogous to $[(C_4H_9N_4)Pt^{II}(CNCH_3)_2]^+$ as seen in Scheme 3.[15,16] The spectroscopic data for the protonated complex shown in Scheme 3 are similar to the data shown in Figure 7. However, the presence of bulky *tert*-butyl groups in the complexes shown in Scheme 3 prevents self-association through Pt··· Pt interactions.

In conclusion, the present work demonstrates the effects of outer sphere interactions in determining the nature and extent of self-association for the planar d^8 cation $[(C_4H_9N_4)Pt^{II}(CNCH_3)_2]^+$. For cationic complexes of this sort, the nature of the anion and its ability to engage in interactions with the cation produce remarkable variations in the structural features of the resulting salts.

Experimental Section

Materials. Solutions of potassium tetrachloroplatinate(II) (Pressure Chemicals) were filtered prior to use. Methyl isocyanide was prepared according to a published procedure.[17] All other reagents were commercially obtained and used as received without further purification. Samples of the Chugaev's salts, $[(C_4H_9N_4)Pt^{II}(CNCH_3)_2](BPh_4)\cdot CH_3OH$, $[(C_4H_9N_4)Pt^{II}(CNCH_3)_2](PF_6)\cdot CH_2Cl_2$, $[(C_4H_9N_4)Pt^{II}(CNCH_3)_2]Cl\cdot 4H_2O$, $[(C_4H_9N_4)Pt^{II}(CNCH_3)_2]Br\cdot 3.5H_2O$, and $[(C_4H_9N_4)Pt^{II}(CNCH_3)_2]Cl\cdot 0.1H_2O$, were prepared by established procedures.[9,10,11,18]

Crystal Growth. $[(C_4H_9N_4)Pt^{II}(CNCH_3)_2](BPh_4)\cdot CH_3OH$. A sample of $[(C_4H_9N_4)Pt^{II}(CNCH_3)_2](BPh_4)\cdot CH_3OH$ was recrystallized from warm methanol to give yellow plates of the methanol solvate. Infrared (hydrocarbon mull): 3444(m), 3318(m), 3053(s), 2256(s){νCN}, 2241(s){νCN}, 1578(s), 1530(s), 1509(s), 1504-(s), 732(s), 707(s) cm^{-1}.

$[(C_4H_9N_4)Pt^{II}(CNCH_3)_2](PF_6)\cdot CH_2Cl_2$. Red blocks which rapidly decomposed (apparently due to loss of dichloromethane) were obtained by diffusion of dichloromethane into an acetonitrile solution of the salt. Infrared (hydrocarbon mull): 3653(m), 3464-(s), 3399(s), 3291(s), 2261(s){νCN}, 2243(s){νCN}, 1582(s), 1536-(s), 1512(s), 1493(s), 841(vs){νPF} cm^{-1}.

$[(C_4H_9N_4)Pt^{II}(CNCH_3)_2]Cl\cdot 4H_2O$. Red needles with a copper metallic sheen were grown over several days by slow diffusion of wet diethyl ether into a concentrated methanolic solution of $[(C_4H_9N_4)Pt^{II}(CNCH_3)_2]Cl\cdot 4H_2O$. Infrared (hydrocarbon mull): 3402(s), 3220(s), 2257(s){νCN}, 2246(s){νCN}, 1594(m), 1581-(m), 1530(m), 1515(m), 1497(m) cm^{-1}.

$[(C_4H_9N_4)Pt^{II}(CNCH_3)_2]Cl\cdot 0.1H_2O$. Dichloromethane was allowed to diffuse slowly into a solution of $[(C_4H_9N_4)Pt^{II}(CNCH_3)_2]Cl\cdot 4H_2O$ in dimethyl sulfoxide. Reddish purple needles with a green metallic sheen were harvested after 5 days. Infrared (hydrocarbon mull): 3380(s), 3220(s), 2256(s){νCN}, 2243(s){νCN}, 1581(m), 1530(m), 1511(m) cm^{-1}.

$[(C_4H_9N_4)Pt^{II}(CNCH_3)_2]Br\cdot 3.5H_2O$. A reddish orange concentrated aqueous solution of the compound was layered in a crystal tube over a saturated aqueous solution of KBr. Red blocks of suitable size grew within 24 h. Infrared (hydrocarbon mull): 3413-(s), 3364(s), 3263(s), 2258(s){νCN}, 2252(s){νCN}, 1588(s), 1530-(m), 1523(m), 1519(m) cm^{-1}.

Physical Measurements. Electronic spectra were recorded on a Cary 17 spectrophotometer or a Hewlett-Packard 8450A diode array spectrophotometer. Measurements of monomer/dimer equilibria for $[(C_4H_9N_4)Pt^{II}(CNCH_3)_2]Cl\cdot 4H_2O$ were made using aqueous 1.00 M potassium phosphate solutions with pH = 7.20. All measurements were made within 5 min of sample preparation, and these solutions appeared to be unchanged for about 15 min after preparation. On longer standing, however, purple or black precipitates, which were not simply salts of $[(C_4H_9N_4)Pt^{II}(CNCH_3)_2]Cl\cdot 4H_2O$, formed. The rate of formation of these decomposition products increased as the concentration of $[(C_4H_9N_4)Pt^{II}(CNCH_3)_2]Cl\cdot 4H_2O$ increased. The spectra of crystalline samples were taken on finely ground solid dispersed in potassium bromide and compressed into a pellet. Conventional fluorescence excitation and emission spectra were recorded on a Jorbin-Yvon Fluoromax-b luminescence spectrophotometer at room temperature and were corrected for lamp and detector effects.

X-ray Crystallography and Data Collection. The crystals were removed from the glass tubes in which they were grown together with a small amount of mother liquor and immediately coated with a hydrocarbon oil on the microscope slide. For $[(C_4H_9N_4)Pt^{II}(CNCH_3)_2](PF_6)\cdot CH_2Cl_2$, the crystals were cooled in dry ice immediately upon removal from the tube in which they were grown in order to minimize loss of dichloromethane. Suitable crystals were mounted on glass fibers with silicone grease and placed in the cold dinitrogen stream of a Bruker SMART CCD with graphite monochromated Mo Kα radiation at 90(2) K. No decay was

(17) Schuster, R. E.; Scott, J. E.; Casanova, J. Jr. *Organic Syntheses*; Wiley and Sons: New York, 1973; Collect. Vol. 5, p 772.
(18) Rouschias, G.; Shaw, B. L. *J. Chem. Soc. A* **1971**, 2097.

observed in 50 duplicate frames at the end of each data collection. Crystal data are given in Table 1.

The structures were solved by direct methods and refined using all data (based on F^2) with the software of SHELXTL 5.1. A semiempirical method utilizing equivalents was employed to correct for absorption.[19] Hydrogen atoms were added geometrically and refined with a riding model.

Acknowledgment. We thank the Petroleum Research Fund (Grant 37056-AC) for support. The Bruker SMART 1000 diffractometer was funded in part by NSF Instrumentation Grant CHE-9808259.

(19) SADABS 2.10, based on a method of R. H. Blessing: Sheldrick, G. M. *Acta Crystallogr., Sect. A* **1995**, *A51*, 33.

Supporting Information Available: Figure S1, S2, and S3 and the derivation of eq 2. X-ray crystallographic files in CIF format for $[(C_4H_9N_4)Pt^{II}(CNCH_3)_2](BPh_4)\cdot CH_3OH$, $[(C_4H_9N_4)Pt^{II}(CNCH_3)_2](PF_6)\cdot CH_2Cl_2$, $[(C_4H_9N_4)Pt^{II}(CNCH_3)_2]Cl\cdot 4H_2O$, $[(C_4H_9N_4)Pt^{II}(CNCH_3)_2]Br\cdot 3.5H_2O$, and $[(C_4H_9N_4)Pt^{II}(CNCH_3)_2]Cl\cdot 0.1H_2O$. This material is available free of charge via the Internet at http://pubs.acs.org.

IC049226J